Content

S1. A simplified schematic diagram of the synthesized CNT@Mn_3O_4 sample.

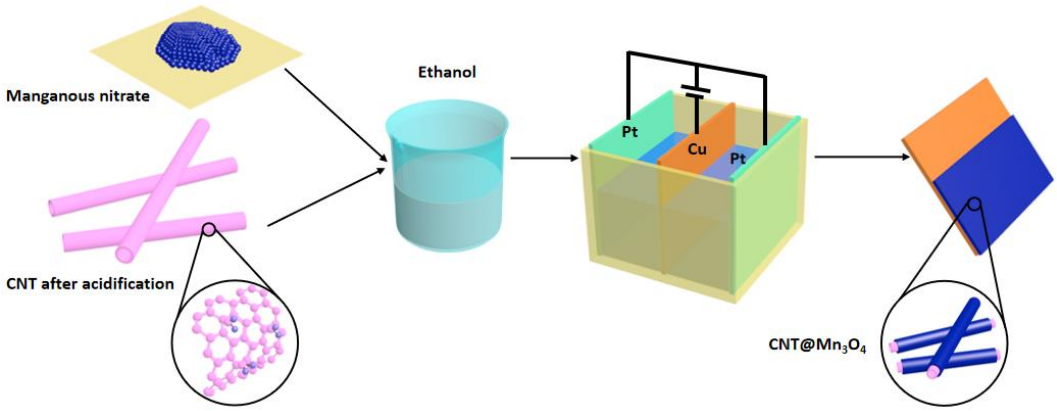

Figure S1. A simplified schematic diagram of the synthesized CNT@Mn_3O_4 sample.

As depicted in Fig. S1, the deposition suspension was prepared by ultrasonically dispersing 13 mg of pretreated CNTs and 120 mg of $Mn(NO_3)_2$ (50% aqueous solution, AR) in 100 mL of absolute ethanol. A rectangular copper foil (30 mm×40 mm) was used as a cathode and a rectangular platinum foil (30 mm×40 mm) as an anode. The copper cathode and platinum anode were kept parallel in the suspension with a plate distance of 10 mm. The deposition experiment was performed at a constant voltage of 50 V and a deposition time of 300 s. In this deposition process, electrophoretic deposition of CNT and cathodic deposition of Mn^{2+} ions occurred synchronously, leading to the one-step formation of a hybrid electrode. After deposition, the as-obtained hybrid electrode was firstly washed with ethanol to remove the residual $Mn(NO_3)_2$

S2. Photos of the as-prepared CNT@Mn_3O_4 sample deposited on copper foil.

Figure S2. Photos of the as-prepared CNT@Mn_3O_4 sample deposited on copper foil.

As shown in Fig. S2, after the sedimentation was completed, the copper foil loaded with composite material was placed in a N_2 atmosphere and calcined at 300 degrees Celsius for 3 hours to obtain the product shown in the figure.

S3. Physical properties and electrochemical LIB cycling data of Mn_3O_4-based nanocomposites.

Electrode materials	Preparation method	Current rate(mAh g^{-1})	Specific capacity (mAh g^{-1})	Number of cycles	Ref.
Mn_3O_4@pGS	Template method	100	770	200	[1]
rGO/Mn_3O_4	Hydrothermal process and others	100	802	100	[2]
Mn_3O_4 microsphere	Hydrothermal process and others	100	640	100	[3]
Mn_3O_4/CP	Thermal decomposition route	100	1005	90	[4]
CNTs@Mn_3O_4	Hydrothermal process and others	500	895	200	[5]
CNT@Mn_3O_4	Electrophoretic deposition	1000	1367	300	This work

Figure S3. Physical properties and electrochemical LIB cycling data of Mn_3O_4-based nanocomposites.

As shown in Table S3, our composite demonstrates an extremely high capacity and cycling stability, and exhibits the best performance compared to other similar composites developed in studies on Mn_3O_4.

References

[1] Wang, B.; Li, F.; Wang, X.; Wang, G.; Wang, H.; Bai, J. Mn_3O_4 nanotubes encapsulated by porous graphene sheets with enhanced electrochemical properties for lithium/sodium-ion batteries. *Chem. Eng. J.* **2019**, *364*, 57–69.

[2] Wang, J.G.; Jin, D.; Zhou, R.; Li, X.; Liu, X.R.; Shen, C.; Xie, K.; Li, B.; Kang, F.; Wei, B. Highly flexible graphene/mn3o4 nanocomposite membrane as advanced anodes for li-ion batteries. *Acs Nano* **2016**, *10*, 6227–6234.

[3] Xu, L.; Chen, X.; Zeng, L.; Liu, R.; Zheng, C.; Qian, Q.; Chen, Q. Synthesis of hierarchical Mn_3O_4 microsphere composed of ultrathin nanosheets and its excellent long-term cycling performance for lithium-ion batteries. *J. Mater. Sci. Mater. Electron*. **2019**, *30*, 3055–3060.

[4] Li, X.; Yue, W.; Li, W.; Zhao, J.; Zhang, Y.; Gao, Y.; Gao, N.; Feng, D.; Wu, B.; Wang, B. Rational design of 3D net-like carbon based Mn_3O_4 anode materials with enhanced lithium storage performance. *New J. Chem.* **2022**, *46*, 13220–13227.

[5] Cao, K. Mn_3O_4 nanoparticles anchored on carbon nanotubes as anode material with enhanced lithium storage. *J. Alloys Compd. Interdiscip. J. Mater. Sci. Solid-State Chem. Phys.* **2021**, *854*, 157176–157179.

S4. (a) Raman spectra and（b）（c）xps of CNT@Mn_3O_4 composite materials.

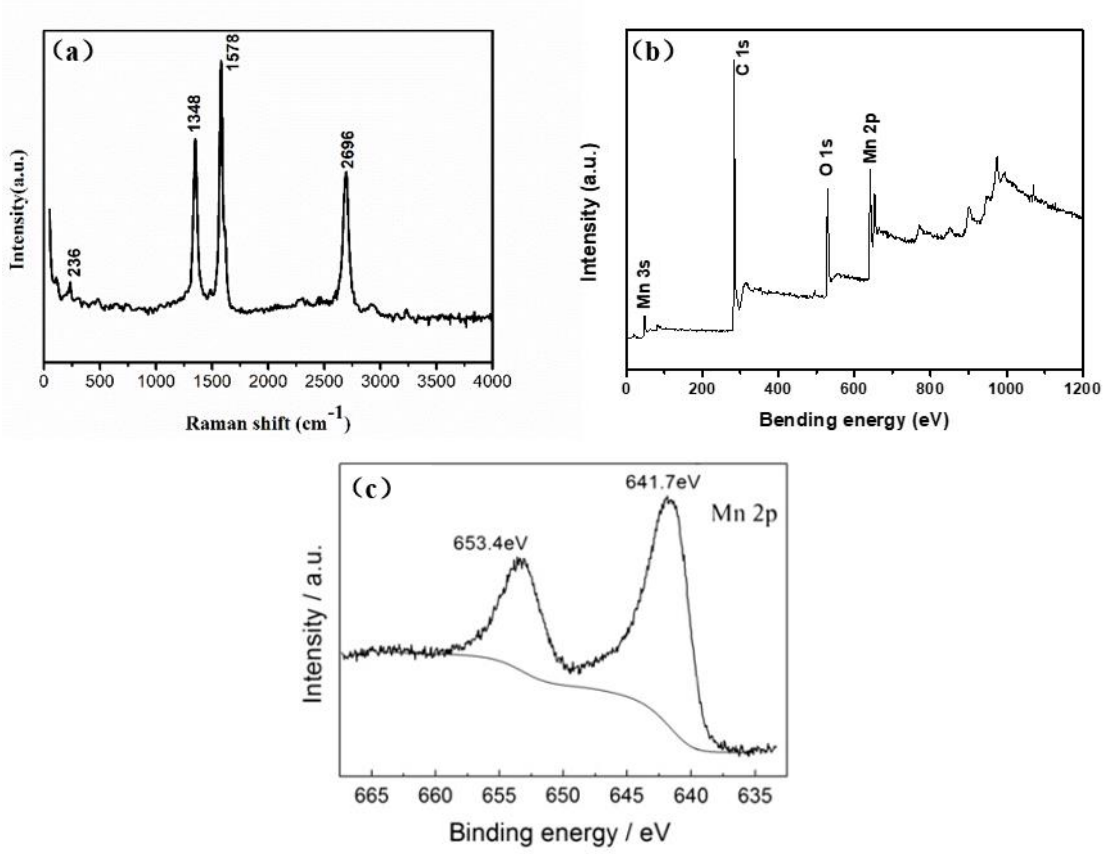

Figure S4. (a) Raman spectra and（b）（c）xps of CNT@Mn_3O_4 composite materials.

Figure S4(a) shows the Raman spectrum of the CNT@Mn_3O_4 composite material, with two strong characteristic peaks at 1348 cm^{-1} and 1578 cm^{-1}. These two peaks correspond to the disordered carbon D band and ordered carbon G band in the carbon nanotubes, respectively. The intensity ratio of the D band to the G band reflects the degree of order in carbon nanotubes, with a higher ratio indicating a lower order degree [1]. The calculated intensity ratio of ID/IG was about 1.32, indicating that the carbon in the prepared sample was in a mixed state of ordered and disordered forms. The peak at 2696 cm^{-1} is the 2D band, which belongs to the double-resonance Raman peak. The red shift indicates that there was an interaction between charges, with the peak position shifting towards a higher frequency, indicating P-type doping; that is, the charge moves from carbon nanotubes to Mn_3O_4. The movement of charges leads to an increase in the hole concentration in carbon nanotubes, which improves their conductivity.

The composition and oxidation state of CNT@Mn_3O_4 were analyzed via XPS spectroscopy, as shown in Figure S4(b). The XPS spectrum shows the presence of Mn (2p, 3s, 3p), O (1s), and C (1s). Figure S4(c) shows the Mn (2p) spectrum, with a

binding energy of Mn 2p3/2 at 641.7 eV. The spin–orbit splitting between Mn $2p_{3/2}$ and Mn $2p_{1/2}$ was 11.7 eV, which is consistent with previous reports on Mn_3O_4 [2,3].

References

[1] Dong, S.; Chang, C.; Liang, Z.; Zhang, Z.; An, L. Electroless deposition of carbon nanotubes doped with nickel and their electrical contact properties. *J. Xi'an Univ.* **2020**, *47*, 88–94.

[2] Varghese, S.P.; Babu, B.; Prasannachandran, R.; Antony, R.; Shaijumon, M.M. Enhanced electrochemical properties of Mn_3O_4/graphene nanocomposite as efficient anode material for lithium ion batteries. *J. Alloys Compd.* **2019**, *780*, 588–596.

[3] Zhang, J.; Chu, R.X.; Chen, Y.L.; Zeng, Y.; Zhang, Y.; Guo, H. Porous carbon encapsulated Mn3O4 for stable lithium storage and its ex-situ XPS study. *Electrochim. Acta* **2019**, *319*, 518–526.

S5. (a) CV curves of the CNT at 10 mV s^{-1};（b）rate performance of the CNT.

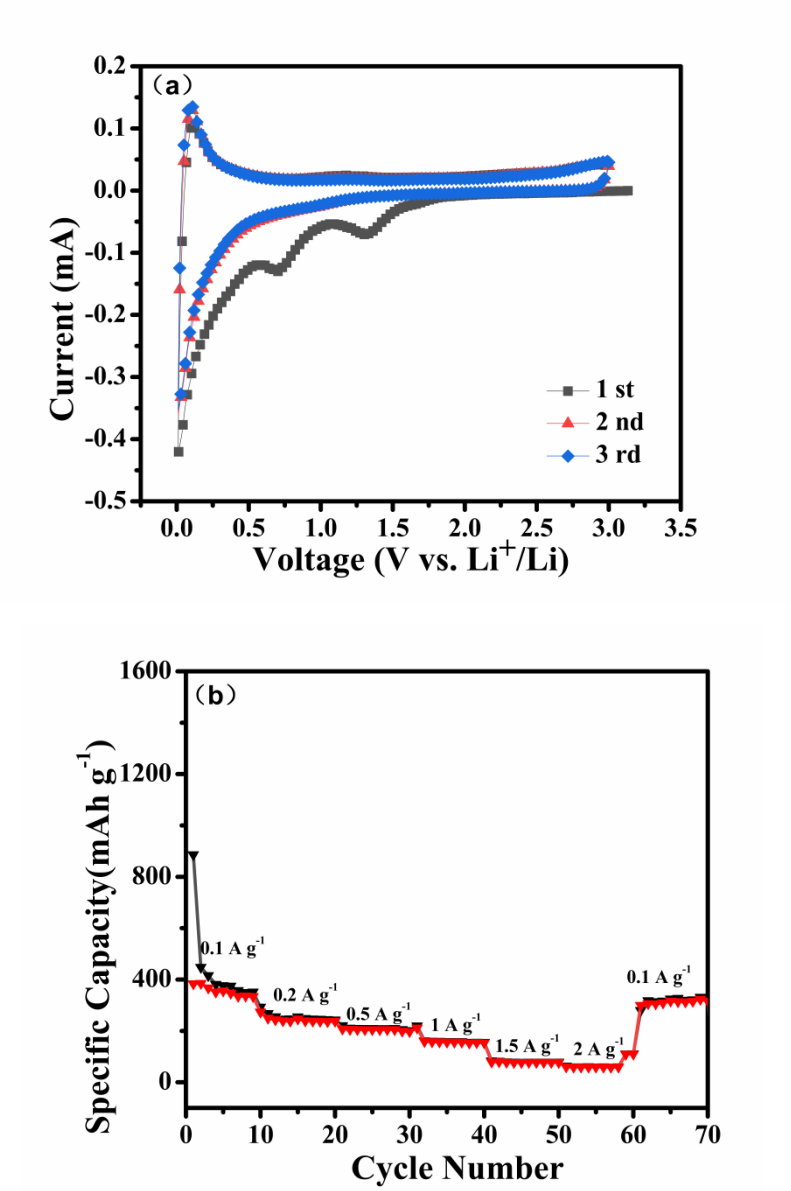

Figure S5. (a) CV curves of the CNT at 10 mV s^{-1};（b）rate performance of the CNT.

By comparing the CV and rate performance of CNT and CNT@Mn_3O_4, it is apparent that the structural advantages of CNT@Mn_3O_4 allow for a higher chemical stability to be maintained.